Light-powered autonomous and directional molecular motion of a dissipative self-assembling system

Light-powered autonomous and directional molecular motion based on a dissipative self-assembling system

Giulio Ragazzon, Massimo Baroncini, Serena Silvi, Margherita Venturi and Alberto Credi*

Photochemical Nanosciences Laboratory, Dipartimento di Chimica "G. Ciamician", Università di Bologna, via Selmi 2, 40126 Bologna, Italy. E-mail: alberto.credi@unibo.it

Biomolecular motors convert energy into directed motion and operate away from thermal equilibrium. The development of dynamic chemical systems that exploit dissipative (non-equilibrium) processes is a challenge in supramolecular chemistry and a premise for the realization of artificial nanoscale motors. Here we report the relative unidirectional transit of a non-symmetric molecular axle through a macrocycle powered solely by light. The molecular machine rectifies Brownian fluctuations by energy and information ratchet mechanisms and can repeat its working cycle under photostationary conditions. The system epitomizes the conceptual and practical elements at the basis of autonomous light-powered directed motion with a minimalist molecular design.

Molecular machines and motors are extensively used by living organisms to perform crucial functions such as transport of substrates and mechanical actuation[1,2]. Synthetic molecular machines[3–5] capable of performing tasks as motor proteins do must exhibit *directionally controlled* motion by dissipating energy from a constant external source in an *autonomous fashion*[3–6]. These aspects are strictly related to the ability of the device to operate away from chemical equilibrium – a condition which is inherent to biochemical systems[7] but represents a formidable challenge for artificial ones[5,6,8]. Despite laboratory demonstration of the potential utility of molecular machines for application in catalysis[9–12], materials science[13–16], ICT[17] and nanomedicine[18], the realization of directional and autonomous molecular movements is a very difficult endeavor, usually tackled with sophisticated chemical structures and/or operation procedures[3–5].

We previously described[19] the directionally controlled transit of a non-symmetric molecular axle through a macrocycle, obtained ratcheting the self-assembly potential energy profile by means of sequential photochemical and chemical stimulation[20]. Building upon these results we now report the relative unidirectional transit of an oriented axle through a macrocyclic ring using light as the sole stimulus[21]. This molecular machine exhibits autonomous behaviour as it can repeat its operation cycle indefinitely under photostationary conditions. Our experiments demonstrate that the device takes advantage of light energy to operate away from equilibrium, thus representing a significant example of dissipative self-assembling system[6]. The results also suggest that both energy and information ratchet mechanisms can account for the rectification of thermal fluctuations brought about by photons[22]. A further element of interest is that the system consists of wholly synthetic unsophisticated compounds and its operation is based on a very efficient, reversible and clean photoreaction, namely, azobenzene $E \leftrightarrows Z$ photoisomerization[23].

Design, preparation, and photoreactivity of the system

The employed molecular components are (Figure 1a) the macrocyclic ring 2,3-dinaphtho[24]crown-8 ether **1**[24] and the molecular axle *E*-**2**$^+$, comprising a photoswitchable *E*-azobenzene unit at one end, a central ammonium recognition site for the macrocycle, and a passive methylcyclopentyl pseudo-stopper at the other end[19]. As shown schematically in Figure 1b, the ring should enter exclusively from the *E*-azobenzene side of the axle for kinetic reasons, affording a pseudorotaxane [**1**$\supset$*E*-**2**]$^+$ in which the macrocycle encircles the recognition site on account of hydrogen bonding interactions between the oxygen atoms and the ammonium centre and, possibly, π-stacking forces involving the naphthalene and azobenzene units[25]. Subsequently, light irradiation converts the *E*-azobenzene unit into the bulkier *Z* form, a process which should also cause a destabilization of the supramolecular complex [**1**$\supset$*Z*-**2**]$^+$ and dethreading of the components. If the extrusion from the ring is faster for the pseudo-stopper of the axle than for its *Z*-azobenzene unit, dethreading should occur preferentially along the same direction originally followed for threading. Reset is obtained by photochemical or thermal conversion of the azobenzene gate back to the *E* isomer, thereby regenerating the starting form of the axle and causing directionally controlled threading once again (Figure 1b).

In the present system, autonomous light-powered cycling[26–29] between the states shown in Figure 1b under steady irradiation is possible because the same photons can trigger both $E \rightarrow Z$ and $Z \rightarrow E$ photoisomerizations, owing to the overlapping absorption spectra and photoreactivity of *E*- and *Z*-azobenzene. Overall, the photoinduced relative unidirectional transit of the axle through the

macrocycle would be obtained according to a flashing energy ratchet mechanism (Figure 1c), in which a single photonic stimulus controls both the relative stabilities of the assembled and disassembled states (i.e., switching) and the relative heights of the kinetic barriers for threading/dethreading over either extremities (i.e., gating)[22].

Directionally controlled threading/dethreading movements

^{1}H NMR Spectra in CD_2Cl_2 (see Figures S3-S4) show that both *E*- and *Z*-**2**$^+$ form 1:1 pseudorotaxane-type complexes with macrocycle **1**. The association of **1** and **2**$^+$ causes also changes in the UV-visible absorption and luminescence spectra; in particular, the intense fluorescence of **1** (λ_{max} = 345 nm) is completely quenched when the ring is complexed by either isomer of axle **2**$^+$. The thermodynamic and kinetic data for self-assembly of these complexes, together with those of the complexes formed by the symmetric model axles **3**$^+$ and *EE*-**4**$^+$ (Figure 1a) with macrocycle **1**, are reported in Table 1 (see also Table S1, Equation S1 and Figures S5-S24). Axles *Z*-**2**$^+$ and *ZZ*-**4**$^+$, as well as their complexes with **1**, can be obtained by exhaustive irradiation of the corresponding *E* isomers at 365 nm; in all cases the *E*→*Z* conversion at the photostationary state is >96%.

Photochemical experiments performed on the [**1**⊃*E*-**2**]$^+$ complex show that the *E*→*Z* isomerization of the azobenzene unit of **2**$^+$ is sensitized upon irradiation in the absorption bands of **1**, indicating that excitation energy is transferred from the naphthalene units of the ring to the *E*-azobenzene moiety of the axle. Such an energy-transfer process also accounts for the emission quenching, as confirmed by the fact that the luminescence is quenched when **1** is complexed by *EE*-**4**$^+$, while it is unaffected in the [**1**⊃**3**]$^+$ complex. Conversely, the photosensitization of the *Z*→*E* transformation in the [**1**⊃*Z*-**2**]$^+$ complex is not efficient because of the poor overlap of the emission spectrum of **1** with the absorption spectrum of the *Z* isomer of the axle. The significant quenching of the emission of **1** in the [**1**⊃*Z*-**2**]$^+$ complex can be ascribed to electron transfer from the photoexcited naphthalene moiety of the ring to the LUMO orbital of the azobenzene axle.

The fact that the threading rate constant for *E*-**2**$^+$ is close to that of *EE*-**4**$^+$ and 25 times faster than that of **3**$^+$ (Table 1, Figure 2a) indicates that axle *E*-**2**$^+$ enters ring **1** almost exclusively (>96%) with its *E*-azobenzene terminus. On the other hand, the rate constant for self-assembly of **1** and *Z*-**2**$^+$ compares with that for threading of **3**$^+$ which, in its turn, is 50 times faster than that for threading of *ZZ*-**4**$^+$. All these observations clearly indicate that *Z*-**2**$^+$ threads the ring with its methylcyclopentyl terminus, and confirm that the *E*⇆*Z* photoisomerization can effectively be used to control the self-assembly kinetics[30].

In contrast with the behaviour of an earlier system[19], the $E \leftrightarrows Z$ photoisomerization of $\mathbf{2}^+$ affects the stability of the resulting pseudorotaxane, as shown by luminescence titration curves (Figure 2b). The association constant with **1** drops from 6.3×10^5 M^{-1} for E-$\mathbf{2}^+$ to 1.7×10^5 M^{-1} for Z-$\mathbf{2}^+$, most likely as a consequence of a diminished π-stacking of the naphthalene units of **1** with the non-planar *Z*-azobenzene moiety. Under typical experimental conditions (1:1 mixture of 50 μM **1** and $\mathbf{2}^+$), exhaustive 365-nm irradiation affords the dethreading of about 15% of the pseudorotaxane species. Hence, the reversible photoisomerization of the axle can be exploited also for switching the system, i.e., change the relative stabilities of the self-assembled and disassembled states (Figure 1c).

The direction of photoinduced dethreading can be determined considering that barriers (or rate constants) for threading with the different termini of a non-symmetric axle give information about the relative height of the corresponding dethreading barriers. On the basis of the threading rate constants for $\mathbf{3}^+$ and ZZ-$\mathbf{4}^+$ with **1** it can be calculated that more than 98% of Z-$\mathbf{2}^+$ axles will enter the macrocycle with the methylcyclopentyl stopper. Therefore it can be concluded that extrusion of the methylcyclopentyl unit is kinetically preferred over *Z*-azobenzene in the dethreading of [**1**⊃*Z*-**2**]$^+$. It should also be noted that the latter process ($k = 4.7\times10^{-6}$ s^{-1}) is faster than the thermal $Z \rightarrow E$ isomerization ($k = 1.6\times10^{-6}$ s^{-1}); these numbers indicate that, on average, the complex should have approximately three dethreading chances before its azobenzene gate is thermally converted back to the *E* configuration. The full reset of the system is determined solely by the $Z \rightarrow E$ isomerization, which restores the original potential energy landscape (Figure 1c) and promotes the re-threading of E-$\mathbf{2}^+$ into **1** preferentially with the azobenzene terminus (Figure 1b), thus completing the operation cycle.

Autonomous operation away from equilibrium

It is well known that for a closed path of reactions at thermal equilibrium, detailed balance – a consequence of microscopic reversibility – states that each individual process has to be at equilibrium, that is, no directional flow can occur[22,31]. In our case, two of the four processes – namely, isomerization of the free and complexed axle (Figure 3, processes 2 and 4) are photochemically driven and hence are not subjected to microscopic reversibility[31–33]. One can define $K_{2,h\nu}$ and $K_{4,h\nu}$ as the ratio of the concentrations of the products and reactants for the respective reactions once the steady state under light irradiation is reached. Our results show that the photostationary states afforded upon irradiation of the free and complexed axle at $\lambda > 400$ nm have the same *E*/*Z* composition. This means that $K_{2,h\nu} = K_{4,h\nu}$ but since $K_1 > K_3$ (the ring associates more strongly with E-$\mathbf{2}^+$ than with Z-$\mathbf{2}^+$, Table 1) detailed balance, as anticipated above, is not

fulfilled (see Figure S1 and Equation S2). In other words, at the steady state the net rates of the individual processes in the closed cycle are equal but nonzero, and the system travels through the cycle one way; in the present case the cycling path (clockwise in Figure 3) is dictated by the fact that $K_1 > K_3$. It is worthwhile to remember that, for the reasons described above, the threading-dethreading processes represented in Figure 3 are directionally controlled, i.e., *E*- and *Z*-**2**$^+$ thread/dethread the ring with their *E*-azobenzene and methylcyclopentyl termini, respectively.

Gaining direct experimental evidence of photostationary cycling, however, is not straightforward because the collective chemical and physical properties of the ensemble exhibit no change at the steady state. On the basis of the above discussion the supply of light energy is expected to cause cycling – that is, to establish a net flux around the cycle in one way even if the concentration of each species remains static – thus bringing the system out of equilibrium. Therefore, a proof for autonomous light driven cycling would be the observation that the concentration reached at the photostationary state for any species involved is not consistent with its expected equilibrium value.[28,34,35]

As the fluorescence of **1** is completely quenched when the ring is complexed by either *E*- or *Z*-**2**$^+$, the fluorescence signal measured under appropriate spectral conditions[36] can be correlated to the amount of uncomplexed macrocycle present in the solution. We therefore monitored the concentration of the free ring in a solution containing **1** and **2**$^+$ kept under steady irradiation at 365 nm. In an optimized experiment, a solution containing 50 μM **1** and 150 μM *E*-**2**$^+$ was let to equilibrate in the dark at 20 °C; the self-assembly of the components was revealed by a strong decrease of the emission intensity. Irradiation of the solution with relatively high intensity (1.7×10^{-6} Einstein min^{-1}) 365-nm light afforded nearly complete $E\rightarrow Z$ conversion, in such a short time (5 min) that the self-assembly equilibria cannot keep up with the photoisomerization changes. In fact, the concentration of the free ring was unchanged within errors after the irradiation, confirming that the dethreading of a fraction of the [**1**⊃*Z*-**2**]$^+$ species, expected because its stability constant is lower than that of [**1**⊃*E*-**2**]$^+$, does not take place on this time scale.

Once the system had been completely photoisomerized (that is, when the absorption spectrum became invariant, see Figures S20-S21), the irradiation was resumed with a lower light intensity (1.0×10^{-7} Einstein min^{-1}) to prevent any photodecomposition effect. A decrease of the concentration of the free macrocycle was observed, which reached a plateau at –6% after ca. 2 h of continuous irradiation (Figure 4a). This observation indicates a degree of complexation even larger than that expected for *E*-**2**$^+$ – that is, the guest form exhibiting the highest affinity for the ring – and it is clearly incompatible with any equilibrium mixture of **1** and (*E*- or *Z*-) **2**$^+$. A control experiment

performed on a solution containing the macrocycle and the deprotonated guest *E*-**2** (lacking the ammonium recognition site and thus unable to associate with **1**) under otherwise identical conditions showed no change in the emission intensity upon prolonged irradiation (Figure 4a), confirming that the observed effect arises from the interplay of photoisomerization and self-assembly processes (Figure 3).

Such an effect can be understood considering that dethreading of [**1**⊃*Z*-**2**]$^+$ through the methylcyclopentyl group is the slowest of all processes of the cycle (Table 1); hence, a larger concentration of this species at the photostationary state with respect to dark equilibrium conditions is expected. In practice, while the cycle operates, reaction 2 (Figure 3) populates the [**1**⊃*Z*-**2**]$^+$ state, characterized by very slow dissociation kinetics, scavenging [**1**⊃*E*-**2**]$^+$ and thus fostering the complexation of *E*-**2**$^+$ generated in reaction 4 with the concomitant decrease of free ring concentration. This mechanism is efficient because, under steady irradiation, light continously and repeatedly triggers both $E \rightarrow Z$ and $Z \rightarrow E$ isomerization.

When the light is switched off, [**1**⊃*Z*-**2**]$^+$ begins to dethread because its concentration is higher than the equilibrium value, and the amount of the free ring initially increases (Figure 4b). As the slow concomitant $Z \rightarrow E$ thermal isomerization regenerates the *E*-isomer, the ring concentration is expected to level off as time goes on. Unfortunately the absorption changes associated with the isomerization prevent an accurate determination of the fluorescence intensity because of the strong reabsorption of the emitted light[36]. Nevertheless, after 20 days in the dark at room temperature – that is, when all the isomerization and self-assembly processes have reached equilibrium – the observed emission intensity is identical to that measured for the equilibrated solution of **1** and *E*-**2**$^+$ before irradiation. This result highlights the full reversibility and a remarkable fatigue resistance of this ensemble.

Energetic and mechanistic considerations

To verify our interpretation of the observed results we performed numeric simulations of the cycle shown in Figure 3 using the experimentally determined values for threading, dethreading, photoisomerization and thermal isomerization rates (Table 1, Figure S2 and Equations S3-S10). The excellent match between the simulation and the measured data points (Figure 4a) confirms the validity of our mechanistic hypotheses.

A few interesting facts can be extracted from the simulation to assess the performance of the cycle (see Equations S11-S13). The cycling rate is 1.7×10^{-10} M s^{-1}, and the efficiency is 2.3×10^{-3} cycles

per photon; that is, about 430 photons need to be absorbed on average to complete a cycle. The product of the rate constants of the clockwise processes divided by the product of the rate constants of the counterclockwise ones (Figure 3) indicates that, on average, the system loops in the "wrong" way (i.e., counterclockwise) once every 160 cycles. The maximum amount of work that could be performed in a cycle, which can be estimated from the free energy change of the system[22,37], is 5.1 k_BT (3.0 kcal mol^{-1} at 20 °C), i.e., about one fourth of the energy provided by ATP hydrolysis. Considering that, under the conditions employed, one cycle uses ca. 430 photons of 365-nm light (78 kcal mol^{-1}), the upper limit for the energy conversion efficiency is 9×10^{-5}.

A closer inspection at the photochemical data (see Table S2) enables a discussion about the mechanisms used by this system to rectify Brownian fluctuations[22]. Firstly, we found that the $E\rightarrow Z$ conversion at the photostationary state upon irradiation at 365 nm is slightly larger for the complex than for the free axle ($K_{2,h\nu} > K_{4,h\nu}$). As the photoisomerization quantum yields are not affected by the presence of the macrocycle, the more efficient $E\rightarrow Z$ transformation in the complex must arise from its slightly higher molar absorption coefficient at 365 nm in comparison with the free axle. The situation is even more interesting when the system is irradiated with light absorbed also by the ring component (e.g., 287 nm). Because excitation energy is efficiently transferred from **1** to *E*-**2**$^+$ but not to *Z*-**2**$^+$ in their respective complexes (and, as noted above, the inherent photoisomerization efficiency of the axle does not change when it is surrounded by the ring), irradiation of the ring-axle mixture at this wavelength generates a photostationary state with a larger *Z*/*E* composition than for the axle alone and, again, $K_{2,h\nu} > K_{4,h\nu}$.

The device operation is based on pure energy ratcheting[22,38] if irradiation is performed with $\lambda > 400$ nm ($K_{2,h\nu} = K_{4,h\nu}$ as discussed above), whereas a contribution from information ratcheting[22,34,35] takes place upon irradiation at 365 or 287 nm, although via different physical phenomena. The ring does not absorb light at 365 nm but its presence enhances the absorption of the *E*-axle, leading to the preferential light-triggered closure of the azobenzene gate in the pseudorotaxane compared to the free axle. On the other hand, the light absorbed by the ring at 287 nm causes the transfer of excitation energy to the *E*-axle – a process that can efficiently occur only if the components are bound – and triggers the $E\rightarrow Z$ isomerization of the latter[34]. In both cases, the information about the location of the ring with respect to the axle can control the gating[31].

Conclusions

We have described a dissipative self-assembling ensemble that uses light energy to perform directed molecular movements in a repetitive fashion out of equilibrium[6]. Although the system as such cannot be used to perform work in a bulk solution[37], it provides a viable route for the construction of rotary motors based on catenanes[39] or linear motors[40] based on polymeric motifs[9,11], capable of moving – and possibly transporting cargos – over long distances. It can also be regarded as a precursor of artificial molecular pumps[38] capable of generating concentration gradients across membranes[41,42,43,44]. To this aim, we are applying the above discussed strategy to three-dimensional macrocycles that can be included in bilayer membranes[45,46] and in which face selective threading is possible[47,48].

Besides practical applications, this system is of high interest because it epitomizes the conceptual and practical elements at the basis of repetitive directionally controlled molecular motion powered by light[22,31,37]. Its minimalist design, facile synthesis, convenient stimulation, and excellent reversibility are essential features to foster further research developments and a fundamental premise for real world applications.

References

1. Jones, R.A.L. *Soft machines: nanotechnology and life*. (Oxford University Press, 2008).

2. Schliwa, M. (Ed.) *Molecular Motors*. (Wiley-VCH, 2003).

3. Balzani, V., Credi, A. & Venturi, M. *Molecular devices and machines - Concepts and perspectives for the nanoworld*. (Wiley-VCH, 2008).

4. Browne, W.R. & Feringa, B. L. Making molecular machines work. *Nat. Nanotechnol.* **1,** 25–35 (2006).

5. Kay, E.R., Leigh, D.A. & Zerbetto, F. Synthetic molecular motors and mechanical machines. *Angew. Chem. Int. Ed.* **46,** 72–191 (2007).

6. Grzybowski, B.A., Wilmer, C.E., Kim, J., Browne, K.P. & Bishop, K.J.M. Self-assembly: from crystals to cells. *Soft Matter* **5,** 1110–1128 (2009).

7. Mann, S. Life as a nanoscale phenomenon. *Angew. Chem. Int. Ed.* **47,** 5306–5320 (2008).

8. Lehn, J.-M. Toward complex matter: supramolecular chemistry and self-organization. *Proc. Natl. Acad. Sci. U. S. A.* **99,** 4763–4768 (2002).

9. Thordarson, P., Bijsterveld, E.J.A., Rowan, A.E. & Nolte, R.J.M. Epoxidation of polybutadiene by a topologically linked catalyst. *Nature* **424,** 915–918 (2003).

10. Wang, J. & Feringa, B.L. Dynamic control of chiral space in a catalytic asymmetric reaction using a molecular motor. *Science* **331,** 1429–1432 (2011).

11. Van Dongen, S.F.M. *et al.* A clamp-like biohybrid catalyst for DNA oxidation. *Nat. Chem.* **5,** 945–51 (2013).

12. Blanco, V., Leigh, D.A., Marcos, V., Morales-Serna, J.A. & Nussbaumer, A.L. A switchable [2]rotaxane asymmetric organocatalyst that utilizes an acyclic chiral secondary amine. *J. Am. Chem. Soc.* **136,** 4905–4908 (2014).

13. Chen, K.-Y. *et al.* Control of surface wettability using tripodal light-activated molecular motors. *J. Am. Chem. Soc.* **136,** 3219–3324 (2014).

14. Vukotic, V.N., Harris, K.J., Zhu, K., Schurko, R.W. & Loeb, S.J. Metal-organic frameworks with dynamic interlocked components. *Nat. Chem.* **4,** 456–460 (2012).

15. Du, G., Moulin, E., Jouault, N., Buhler, E. & Giuseppone, N. Muscle-like supramolecular polymers: integrated motion from thousands of molecular machines. *Angew. Chem. Int. Ed.* **51,** 12504–12508 (2012).

16. Iamsaard, S. *et al.* Conversion of light into macroscopic helical motion. *Nat. Chem.* **6,** 229–235 (2014).

17. Coskun, A. *et al.* High hopes: can molecular electronics realise its potential? *Chem. Soc. Rev.* **41,** 4827–4859 (2012).

18. Li, Z., Barnes, J.C., Bosoy, A., Stoddart, J.F. & Zink, J.I. Mesoporous silica nanoparticles in biomedical applications. *Chem. Soc. Rev.* **41,** 2590–2605 (2012).

19. Baroncini, M., Silvi, S., Venturi, M. & Credi, A. Photoactivated directionally controlled transit of a non-symmetric molecular axle through a macrocycle. *Angew. Chem. Int. Ed.* **51,** 4223–4226 (2012).

20. Haberhauer, G. A molecular four-stroke motor. *Angew. Chem. Int. Ed.* **50,** 6415–6418 (2011).

21. Li, H. *et al.* Relative unidirectional translation in an artificial molecular assembly fueled by light. *J. Am. Chem. Soc.* **135,** 18609–18620 (2013).

22. Astumian, R.D. Design principles for Brownian molecular machines: how to swim in molasses and walk in a hurricane. *Phys. Chem. Chem. Phys.* **9,** 5067–5083 (2007).

23. Bandara, H.M.D. & Burdette, S.C. Photoisomerization in different classes of azobenzene. *Chem. Soc. Rev.* **41,** 1809–1825 (2012).

24. Davidson, G.J.E., Loeb, S.J., Passaniti, P., Silvi, S. & Credi, A. Wire-type Ruthenium (II) complexes with terpyridine-containing [2]rotaxanes as ligands: Synthesis, characterization, and photophysical properties. *Chem. - A Eur. J.* **12,** 3233–3242 (2006).

25. Ashton, P.R. *et al.* Dialkylammonium ion/crown ether complexes: the forerunners of a new family of interlocked molecules. *Angew. Chem. Int. Ed. Engl.* **34,** 1865–1869 (1995).

26. Koumura, N., Zijlstra, R.W., van Delden, R.A., Harada, N. & Feringa, B.L. Light-driven monodirectional molecular rotor. *Nature* **401,** 152–155 (1999).

27. Klok, M. *et al.* MHz unidirectional rotation of molecular rotary motors. *J. Am. Chem. Soc.* **130,** 10484–10485 (2008).

28. Geertsema, E.M., van der Molen, S.J., Martens, M. & Feringa, B.L. Optimizing rotary processes in synthetic molecular motors. *Proc. Natl. Acad. Sci. U. S. A.* **106,** 16919–16924 (2009).

29. Balzani, V. *et al.* Autonomous artificial nanomotor powered by sunlight. *Proc. Natl. Acad. Sci. U. S. A.* **103,** 1178–1183 (2006).

30. Baroncini, M., Silvi, S., Venturi, M. & Credi, A. Reversible photoswitching of rotaxane character and interplay of thermodynamic stability and kinetic lability in a self-assembling ring-axle molecular system. *Chem. - A Eur. J.* **16,** 11580–11587 (2010).

31. Astumian, R.D. Microscopic reversibility as the organizing principle of molecular machines. *Nat. Nanotechnol.* **7,** 684–688 (2012).

32. Lehn, J.-M. Conjecture: imines as unidirectional photodriven molecular motors-motional and constitutional dynamic devices. *Chem. - A Eur. J.* **12,** 5910–5915 (2006).

33. Greb, L. & Lehn, J.-M. Light-driven molecular motors: Imines as four-step or two-step unidirectional rotors. *J. Am. Chem. Soc.* **136,** 13114–13117 (2014).

34. Serreli, V., Lee, C.-F., Kay, E.R. & Leigh, D.A. A molecular information ratchet. *Nature* **445,** 523–527 (2007).

35. Alvarez-Pérez, M., Goldup, S.M., Leigh, D.A. & Slawin, A.M.Z. A chemically-driven molecular information ratchet. *J. Am. Chem. Soc.* **130,** 1836–1838 (2008).

36. Credi, A. & Prodi, L. Inner filter effects and other traps in quantitative spectrofluorimetric measurements: Origins and methods of correction. *J. Mol. Struct.* **1077,** 30–39 (2014).

37. Coskun, A., Banaszak, M., Astumian, R.D., Stoddart, J.F. & Grzybowski, B.A. Great expectations: can artificial molecular machines deliver on their promise? *Chem. Soc. Rev.* **41,** 19–30 (2012).

38. Chatterjee, M.N., Kay, E.R. & Leigh, D.A. Beyond switches: ratcheting a particle energetically uphill with a compartmentalized molecular machine. *J. Am. Chem. Soc.* **128,** 4058–4073 (2006).

39. Hernández, J.V., Kay, E.R. & Leigh, D.A. A reversible synthetic rotary molecular motor. *Science* **306,** 1532–1537 (2004).

40. Von Delius, M., Geertsema, E.M. & Leigh, D.A. A synthetic small molecule that can walk down a track. *Nat. Chem.* **2,** 96–101 (2010).

41. Steinberg-Yfrach, G. *et al.* Conversion of light energy to proton potential in liposomes by artificial photosynthetic reaction centres. *Nature* **385,** 239–241 (1997).

42. Bennett, I.M. *et al.* Active transport of Ca^{2+} by an artificial photosynthetic membrane. *Nature* **420,** 398–401 (2002).

43. Zhang, H. *et al.* Bioinspired artificial single ion pump. *J. Am. Chem. Soc.* **135,** 16102–16110 (2013).

44. Xie, X., Crespo, G.A., Mistlberger, G. & Bakker, E. Photocurrent generation based on a light-driven proton pump in an artificial liquid membrane. *Nat. Chem.* **6,** 202–207 (2014).

45. Arduini, A. *et al.* Self-assembly of a double calix[6]arene pseudorotaxane in oriented channels. *Chem. - A Eur. J.* **14,** 98–106 (2008).

46. Bussolati, R. *et al.* Hierarchical self-assembly of amphiphilic calix[6]arene wheels and viologen axles in water. *Org. Biomol. Chem.* **11,** 5944–5953 (2013).

47. Arduini, A. *et al.* Towards controlling the threading direction of a calix[6]arene wheel by using nonsymmetric axles. *Chem. - A Eur. J.* **15,** 3230–3242 (2009).

48. Arduini, A. *et al.* Toward directionally controlled molecular motions and kinetic intra- and intermolecular self-sorting: threading processes of nonsymmetric wheel and axle components. *J. Am. Chem. Soc.* **135,** 9924–9930 (2013).

Acknowledgments

This work was supported by the Italian Ministry of Education, University and Research (PRIN 2010CX2TLM) and the University of Bologna (FARB SLaMM project). We thank Francesco Zerbetto and Dean Astumian for discussions.

Authors contributions

M.B. synthesized the compounds; G.R., S.S. and M.B. performed the physico-chemical experiments; G.R. carried out numerical simulations; A.C. conceived the project and wrote the paper. M.V. discussed the results and commented on the manuscript together with all authors.

Additional information

Supplementary information accompanies this paper at www.nature.com/naturenanotechnology. Reprints and permission information is available online at http://npg.nature.com/reprintsandpermissions/. Correspondence and requests for materials should be addressed to A.C.

Competing financial interests

The authors declare no competing financial interests.

Table 1. Kinetic and thermodynamic data for the self-assembly of the investigated complexes (dichloromethane, 20 °C).

Complex	K [a] (M^{-1})	$-\Delta G°$ [b] (kcal mol^{-1})	k_{in} [c] (M^{-1} s^{-1})	$\Delta G^{‡}_{in}$ [d] (kcal mol^{-1})	k_{out} (s^{-1})	$\Delta G^{‡}_{out}$ [d] (kcal mol^{-1})
[**1**⊃*E*-**2**]$^+$	6.3×10^5	7.8	54	14.8	2.2×10^{-5} [c] 8.6×10^{-5} [e]	23.4
[**1**⊃*Z*-**2**]$^+$ [f]	1.7×10^5	7.0	0.81	17.3	4.7×10^{-6} [e]	24.3
[**1**⊃**3**]$^+$	3.2×10^4	6.0	2.2	16.7	3.8×10^{-5} [c] 6.9×10^{-5} [e]	23.1
[**1**⊃*EE*-**4**]$^+$	$>10^7$	>9.4	55	14.8	$<5.5\times10^{-6}$ [e]	>24
[**1**⊃*ZZ*-**4**]$^+$ [f]	[g]	[g]	3.9×10^{-2} [h]	19.0	[i]	[i]

[a] Determined by luminescence or absorption titrations. [b] Free energies of association ($\Delta G°$), calculated from the K values by using the expression $\Delta G° = -RT \ln K$. [c] Determined by UV-vis absorption or luminescence spectroscopy. [d] Free energies of activation for the threading ($\Delta G^{‡}_{in}$) and dethreading ($\Delta G^{‡}_{out}$) processes, calculated by using the relationships $\Delta G^{‡}_{in} = -RT \ln(k_{in}h / kT)$ and $\Delta G^{‡}_{out} = -RT \ln(k_{out}h / kT)$, respectively, where R, h and k correspond to the gas, Planck and Boltzmann constants, respectively. [e] Calculated from the k_{in} and K values by using the expression $k_{out} = k_{in} / K$. [f] Obtained upon exhaustive irradiation of the corresponding *E*- isomer at 365 nm; the $E \rightarrow Z$ conversion yield at the photostationary state was >96% [g] Not measured because equilibrium cannot be reached before substantial thermal $Z \rightarrow E$ back isomerization occurs. [h] Estimated from the initial part of the time-dependent luminescence changes upon mixing **1** and *ZZ*-**4**$^+$, after deconvolution of the contribution of $Z \rightarrow E$ isomerization and threading from the *E*-azobenzene terminus. [i] Not determined.

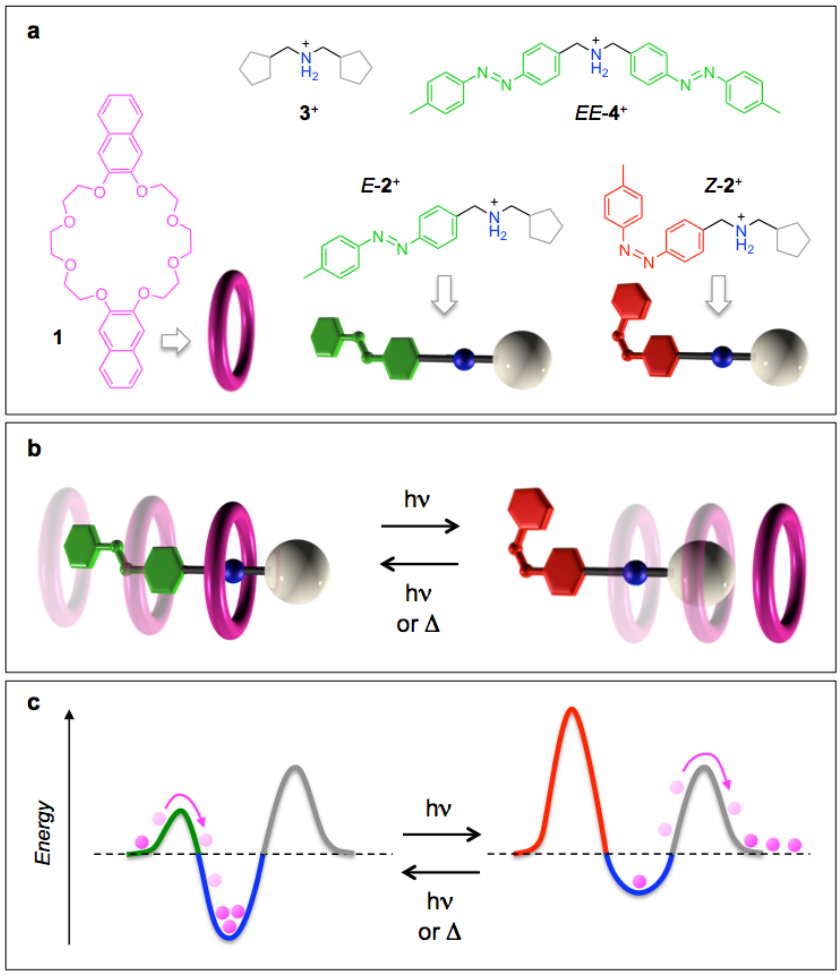

Figure 1. Design and operation of the system. (a) Structure formulas, with cartoon representation, of macrocycle **1**, non-symmetric axles *E*- and *Z*-**2**$^{+}$, and symmetric model axles **3**$^{+}$ and *EE*-**4**$^{+}$. (b) Schematics representation of the relative unidirectional translations of the ring and axle components triggered by light. (c) Simplified potential energy curves (free energy versus ring-axle distance) for the states shown in (b), illustrating how periodic modulation of the energy barriers and wells can produce directional and repetitive threading-dethreading movements.

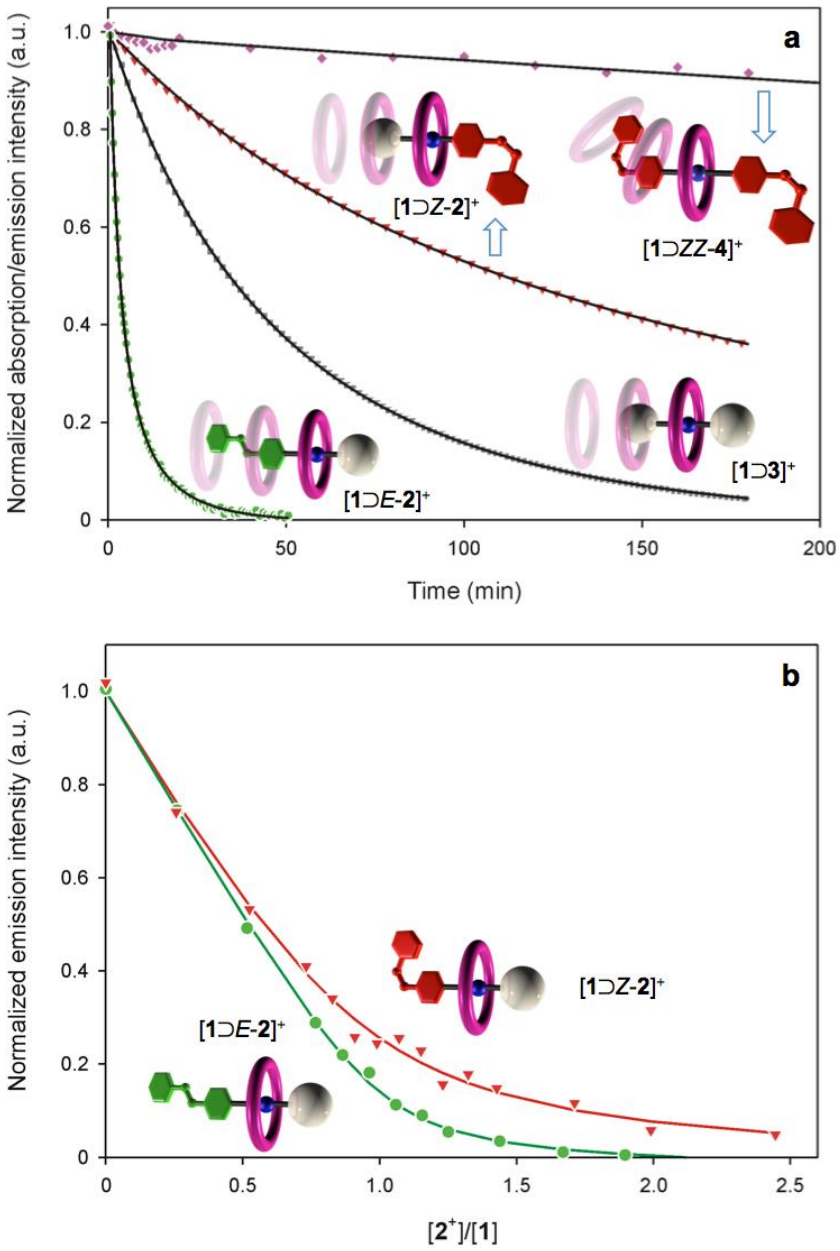

Figure 2. Kinetic and thermodynamic characterization of the self-assembly process. (a) Time-dependent luminescence or absorption changes associated with the self-assembly of the complexes studied in this work. The data corresponding to threading of [**1**⊃*EE*-**4**]$^+$ are not shown because they are fully overlapped with those for threading of [**1**⊃*E*-**2**]$^+$. The full lines represent the data fitting according to a kinetic model consisting of a second-order threading and an opposed first-order dethreading. Conditions: CH_2Cl_2, 20 °C, 100 μM fo each component. (b) Titration curves, obtained from luminescence data, observed upon addition of either *E*-**2**$^+$ or *Z*-**2**$^+$ to a 54 μM solution of **1** in CH_2Cl_2 at 20 °C. The full lines represent the data fitting according to a 1:1 binding model. In all cases, excitation was performed at 272 nm.

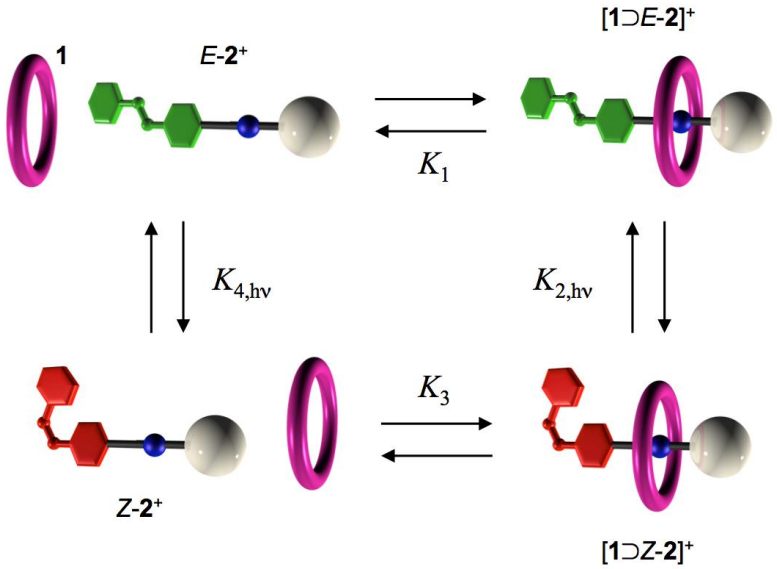

Figure 3. Square cycle of chemical and photochemical reactions representing the operation of the system. Horizontal and vertical arrows denote the self-assembly equilibria and photochemical isomerization reactions, respectively. The indicated parameters refer to the reactions read from left to right and from top to bottom.

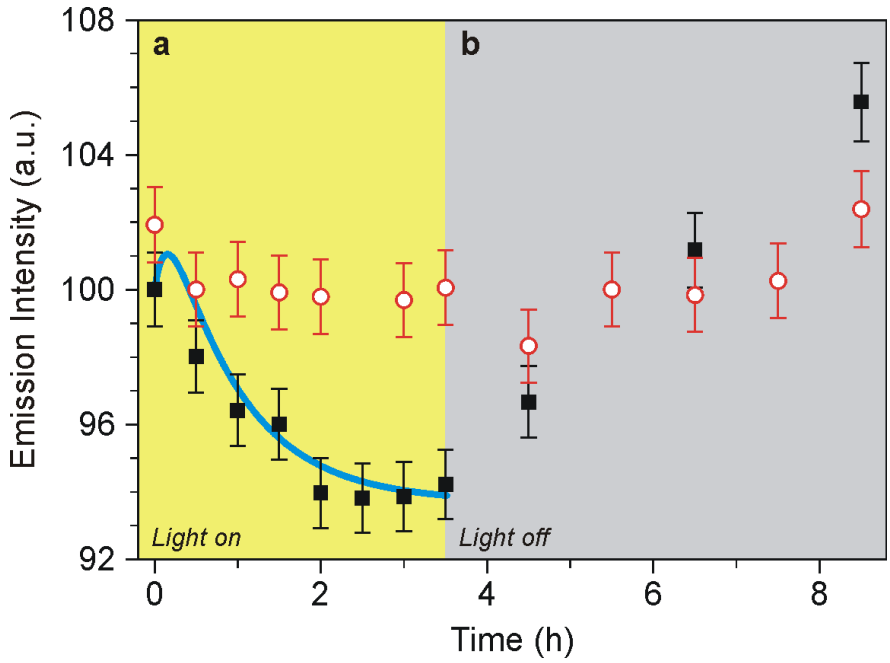

Figure 4. Observation of photostationary cycling of the system away from equilibrium. (a) Fluorescence intensity values of uncomplexed macrocycle **1** upon prolonged 365-nm irradiation of a mixture of ring and axle at the $E \leftrightarrows Z$ photostationary state in CH_2Cl_2 at 20 °C (black squares). The solution was deoxygenated to exclude photodecomposition effects and was prepared by mixing 50 μM **1** and 150 μM *E*-**2**$^+$ (98% complexation of **1**) followed by exhaustive irradiation at 365 nm (99% $E \rightarrow Z$ conversion after 5 min). The empty circles show the fluorescence intensity values in an identical experiment in which the deprotonated axle **2**, lacking the ammonium center and thus unable to associate with **1**, is used in place of **2**$^+$. The full line is a computer simulation of the process, based on the scheme shown in Figure 3 and performed by using the experimentally determined values for threading, dethreading, photoisomerization and thermal isomerization rates. (b) Luminescence changes observed in the experiments described in (a) after irradiation at 365 nm has been switched off. Significant absorption changes, due to $Z \rightarrow E$ thermal isomerization, are observed; inner filter effects prevent the analysis of data points after ca. 8 h. In all cases, excitation was performed at 365 nm. The error bars represent the standard deviation of the luminescence intensity measurement under the adopted experimental conditions. See the text for more details.